Journal of Applied Physics

Repairing the surface of InAs-based topological heterostructures

Cite as: J. Appl. Phys. **128**, 114301 (2020); https://doi.org/10.1063/5.0014361
Submitted: 19 May 2020 . Accepted: 15 August 2020 . Published Online: 15 September 2020

S. J. Pauka, J. D. S. Witt, C. N. Allen, B. Harlech-Jones, A. Jouan, G. C. Gardner, S. Gronin, T. Wang, C. Thomas, M. J. Manfra, J. Gukelberger, J. Gamble, D. J. Reilly, and M. C. Cassidy

Journal of Applied Physics ARTICLE scitation.org/journal/jap

Repairing the surface of InAs-based topological heterostructures

Cite as: J. Appl. Phys. **128**, 114301 (2020); doi: 10.1063/5.0014361
Submitted: 19 May 2020 · Accepted: 15 August 2020 ·
Published Online: 15 September 2020

S. J. Pauka,[1,a)] J. D. S. Witt,[1] C. N. Allen,[2] B. Harlech-Jones,[1] A. Jouan,[1] G. C. Gardner,[3,4] S. Gronin,[3,4] T. Wang,[3,4] C. Thomas,[3,4] M. J. Manfra,[3,4,5,6] J. Gukelberger,[7] J. Gamble,[7] D. J. Reilly,[1,2] and M. C. Cassidy[2]

AFFILIATIONS

[1]ARC Centre of Excellence for Engineered Quantum Systems, School of Physics, The University of Sydney, Sydney, NSW 2006, Australia
[2]Microsoft Quantum Sydney, The University of Sydney, Sydney, NSW 2006, Australia
[3]Birck Nanotechnology Center, Purdue University, West Lafayette, Indiana 47907, USA
[4]Microsoft Quantum Purdue, Purdue University, West Lafayette, Indiana 47907, USA
[5]Department of Physics and Astronomy, Purdue University, West Lafayette, Indiana 47907, USA
[6]School of Materials Engineering and School of Electrical and Computer Engineering, Purdue University, West Lafayette, Indiana 47907, USA
[7]Microsoft Quantum, One Microsoft Way, Redmond, Washington 98052, USA

[a)]**Author to whom correspondence should be addressed:** sebastian.pauka@sydney.edu.au

ABSTRACT

Candidate systems for topologically-protected qubits include two-dimensional electron gases (2DEGs) based on heterostructures exhibiting a strong spin–orbit interaction and superconductivity via the proximity effect. For InAs- or InSb-based materials, the need to form shallow quantum wells to create a hard-gapped *p*-wave superconducting state often subjects them to fabrication-induced damage, limiting their mobility. Here, we examine scattering mechanisms in processed InAs 2DEG quantum wells and demonstrate a means of increasing their mobility via repairing the semiconductor–dielectric interface. Passivation of charged impurity states with an argon–hydrogen plasma results in a significant increase in the measured mobility and reduction in its variance relative to untreated samples, up to 45 300 $cm^2/(V\,s)$ in a 10 nm deep quantum well.

I. INTRODUCTION

Interest in proximitized InAs- and InSb-2DEGs has intensified recently due to their potential application in spintronics[1] and topological quantum computation.[2,3] These materials can exhibit superconductivity via the proximity effect,[4] induced by the presence of aluminum deposited on their surface, which strongly couples to the quantum well. The induced superconductivity combined with strong SOI (and a large Landé g-factor) results in the formation of Majorana zero modes (MZMs), now observed in both nanowires[5,6] and 2DEGs,[7,8] at the boundaries of the topological superconductor.[9–11] Interest in MZMs, which are emergent quasi-particles hypothesized to have non-Abelian exchange statistics, stems from their potential to provide topological protection to quantum information.[12]

Early experimental platforms for realizing MZMs in both nanowires and 2DEGs utilized superconductors deposited *ex situ*; however, these systems demonstrated a significant sub-gap density of states that obscured the signatures of the MZM.[13,14] Alternatively, *in situ* deposition of a superconductor, such as epitaxially growing aluminum directly after semiconductor growth, results in a significant improvement in the quality of the superconducting gap,[15,16] and the realization of a quantized zero-bias peak.[17] *In situ* deposition poses additional fabrication challenges, however, as the Al must be removed to define the topological region of the device. Removal via a wet-etch solution selective to Al is a highly exothermic reaction that results in damage to the surface of the semiconductor. This damage manifests as increased

roughness and induced impurities, lowering the mobility of the 2DEG[18] and compromising the fragile induced p-wave superconducting pairing.[19,20] Furthermore, since the length scale over which hard-gap superconductivity is maintained across a clean interface is set by the height and thickness of the barrier,[14] burying the 2DEG deep in the heterostructure is not feasible.[4] Taken together, these aspects point to a need to develop new fabrication techniques that maintain or repair defects introduced at the surface.

Here, we investigate the scattering mechanisms that reduce mobility in shallow (In,Al)As/InAs/(In,Ga)As 2DEG heterostructures following wet-etch of the proximitizing superconductor. We demonstrate that the mobility can be increased and the variance of the mobility is reduced by exposing the sample to an *in situ* ArH plasma, prior to deposition of a protective ALD (atomic layer deposition) grown Al_2O_3 coating. We compare the mobility of these to samples exposed to an *in situ* trimethylaluminum (TMA) pre-treatment, or to samples without any pre-treatment, prior to oxide growth. By studying the mobility and density of the treated samples, we show that surface scattering is the dominant mechanism for reduced mobility in shallow 2DEG samples, consistent with previous measurements[21] and that the reduction of the density of charged surface states leads to increased peak mobility.

II. EXPERIMENT

The devices are fabricated from an undoped $In_{0.9}Al_{0.1}As/InAs/In_{0.81}Ga_{0.19}As$ quantum well grown 10 nm below the surface on a 2 in. (100) InP substrate.[22] An 8 nm Al layer is grown epitaxially on the surface of the heterostructure directly following the semiconductor growth and is used to induce superconductivity in the 2DEG via the proximity effect.[23] On each sample, a Hall bar geometry is defined using a dilute phosphoric acid etch, and Al is selectively removed over the Hall bar with an aluminum wet etch (Transene type-D). Contact to the 2DEG is made using sections of un-etched Al, which forms an ohmic contact. The surface is then treated using either TMA as a reducing agent to remove the native oxide[24,25] or with a ArH plasma to terminate charged impurity states,[26] and without breaking vacuum, a 10 nm Al_2O_3 oxide is grown via ALD at 200 °C, using a TMA precursor and either H_2O or O_3 as an oxidizing agent. Finally, a 150 nm Ti/Au gate is evaporated on the surface of the Hall bar to allow the electron density of the samples to be varied. Further details of the fabrication are contained in the supplementary material. A cross-sectional schematic of the Hall bar is given in Fig. 1(a). For each treatment/oxidizer pair, we fabricate two samples, one taken from within 1 in. of the center of the wafer (denoted "near"), the other taken from the outer 1 in. ring (denoted "far"), in order to account for variation in mobility as a function of distance from the center of the wafer.[27] A full list of tested sample parameters is given in Table I. We note that despite the higher quality of ALD oxides grown at higher temperatures, at temperatures higher than 250 °C, diffusion of In and As occurs, and above 300 °C In begins to precipitate out of the substrate due to the desorption of As.[28]

Charge density and band edge calculations for this material stack are shown in Fig. 1(c). The electrostatic calculations are performed assuming a top gate being placed 10 nm from the surface of the semiconductor, separated by a layer of Al_2O3. As the model does not account for charged impurities at the surface, a positive top gate voltage must be simulated in order to accumulate electrons in the quantum well. This leads to an offset between the simulated and measured sheet density. The evolution from the single- to double-well regime is visible by $V_{TG} = 1.0$ V, leading to the emergence of a second subband at a density of 1.3×10^{12} cm^{-2} (see the supplementary material).

Measurements were carried out in a dilution refrigerator with a base temperature of 7 mK. A Cryo-CMOS based multiplexer is used to allow simultaneous measurement of up to 10 Hall bars in a single cooldown.[29] Magnetotransport measurements were performed to extract electron densities and mobilities using conventional AC lock-in techniques, with a 10 nA constant current. A representative Hall bar is shown in Fig. 1(b), with longitudinal (R_{xx}) and transverse (R_{xy}) resistance measured simultaneously. Three measurement points are defined around the edge of the Hall bar, indicated with blue, red, and black dots, allowing multiple independent measurements of mobility and density to be made on each sample, from which statistics on each treatment are gathered. Hall bars were oriented at 45° to the (011) and (01$\bar{1}$) plane normals to remove the effects of any anisotropy along different crystallographic axes.[30,31] For each sample, density and mobility are extracted as the top gate is swept. A representative measurement is shown for sample B, taken from near the center of the growth wafer, in Fig. 1(d). Mobility is extracted at 0.05 T, which is a sufficiently large offset to ensure we are no longer on the weak-antilocalization peak. For this sample, a peak value for mobility is extracted of 33 400 cm^2/(V s) at a density of 8.73×10^{11} cm^{-2}, corresponding to a gate voltage of $V_{TG} = -0.27$ V, indicated by the red point in Fig. 1(d).

We can attribute different dominant scattering mechanisms to various ranges of the density.[32–34] As the density increases from zero, scattering is predominantly caused by scattering off background impurities distributed through the heterostructure.[35] Increased screening of impurities as the density is increased leads to an increase in mobility. As the gate voltage and density is further increased, the mobility is seen to peak, before reducing with increasing density. Increasing top gate voltage causes the distribution of electrons in the quantum well to shift toward the surface,[36,37] and surface scattering becomes dominant over the increased impurity screening with higher density, leading to the decrease in mobility observed at higher densities. We emphasize that at this point, the charge distribution remains confined to the quantum well.

The subband occupation can be extracted from magnetotransport measurements at high magnetic fields. Figure 2(a), shows a Landau fan for sample B measured in a second cooldown, plotting R_{xx} as V_{TG} and B are swept. The onset of the second subband population occurs at a density of 1.25×10^{12} cm^{-2} and at $V_{TG} = -0.16$ V and is marked by the black arrow on Fig. 2(a), visible as a change in the slope of the location of Landau levels as a function of gate voltage and magnetic field.[38,39] This value is in close agreement with the extracted theoretical value of 1.3×10^{12} cm^{-2}. The onset of the second subband population is also visible as a kink in the mobility as a function of V_{TG}, indicated by the black arrow in Fig. 1(d).

The sample shows significantly different magnetotransport behavior when the first and second subbands are occupied. When the top gate is tuned to the value that maximizes mobility at low

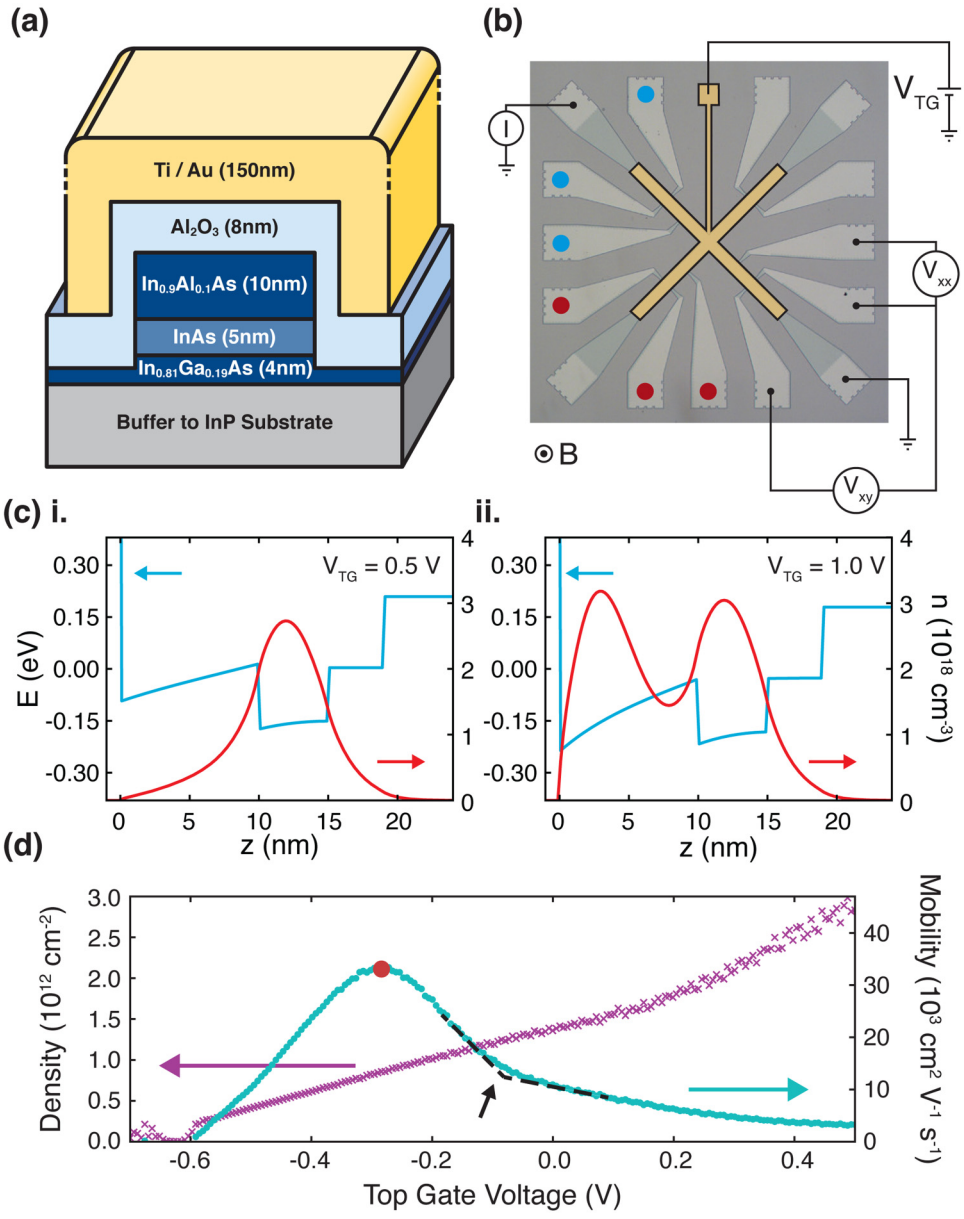

FIG. 1. (a) Cross section of a shallow (In,Al)As/InAs/(In,Ga)As quantum well after removal of epitaxially grown aluminum. A protective layer of Al_2O_3 is grown along with a 150 nm Ti/Au surface gate which is used to tune the electron density. (b) False color micrograph and schematic of the experimental setup showing one combination of current and voltage contacts. Red and blue dots indicate alternative measurement points. (c) Charge distribution (red) and conduction band edge (blue) calculations for a simulated top gate voltage of (i) $V_{TG} = 0.5$ V and (ii) $V_{TG} = 1.0$ V. (d) Density (violet) and mobility (cyan) extracted from sample B using magnetoconductance measurements as the top gate is swept. The red mark indicates the location of peak mobility. The black arrow indicates the location of the onset of the second subband filling. Dashed black lines show the slope of the mobility prior to and following the onset of second subband filling and are included as guides to the eye.

magnetic fields and only a single subband is occupied, well resolved Hall plateaus are observed from $\nu = 10$ onward with the Hall resistivity quantized to within 0.11% of the theoretical value at $\nu = 6$, and a vanishing longitudinal resistance of $R_{xx} = 2.4\,\Omega/\square$. No Shubnikov–de Haas oscillations are observed. In contrast, when the second subband is occupied at $V_{TG} = 0$ V [Fig. 2(c)], clear Shubnikov–de Haas oscillations are visible from 1.5 T to 6 T, despite the much lower mobility of the sample at this point. This is

TABLE I. A full listing of sample growth parameters that were tested. Two surface treatments (TMA reduction and ArH plasma passivation) and two oxidizers (H_2O and O_3) are tested to find their effect on sample mobility. Each treatment and oxidizer pair are measured on two chips, one taken from the center of the growth wafer, the other from near the edge, in order to account for the effect of distance from the center of the wafer on mobility.

Sample	Treatment	Precursor/oxidizer
A	No treatment	TMA/H_2O
B	TMA reduction	TMA/H_2O
C	TMA reduction	TMA/O_3
D	ArH plasma passivation	TMA/H_2O
E	ArH plasma passivation	TMA/O_3

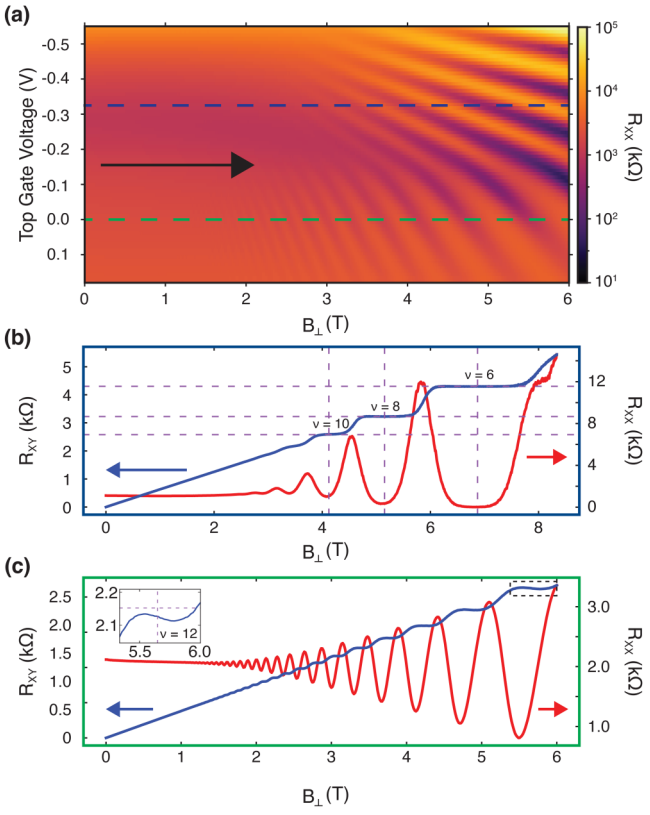

FIG. 2. (a) The Landau fan for sample B. The black arrow marks the onset of the second subband population, indicated by a change in the slope of the Landau levels as a function of magnetic field and top gate voltage. The location of peak mobility is indicated by the blue dashed line. (b) Magnetoresistance taken at the point of highest mobility on sample B. Well resolved Hall plateaus are observed, starting from $\nu = 10$ (see main text for details). (c) Magnetoresistance measurements of sample B to high field, taken at $V_{TG} = 0$ V. Hall plateaus show an oscillation characteristic of parallel conduction paths.

caused by the increased screening of the impurity potential by the electrons of the second subband and has been observed in measurements of low-mobility GaAs 2DEGs.[40] Further evidence of second subband population is seen in the Hall plateaus which are not well quantized and exhibit an oscillatory behavior [inset Fig. 2(c)], an effect attributed to parallel transport in the second subband.

III. SURFACE TREATMENTS AND OXIDE GROWTH

The native oxide layer in both GaAs and InAs is known to contain a large number of charged defects,[41,42] caused by unpaired As atoms within the oxide formed by an excess of As during the oxidation of In and Ga.[43,44] These defects act as scattering sites at the surface of the wafer and limit the mobility of samples above a certain density. Reducing the concentration of surface scattering sites through chemical treatment prior to dielectric deposition provides a clear pathway to increasing the sample mobility.

The first approach that we examine is the removal of the native oxide through reduction by TMA.[41,45–47] TMA is known to remove the surface oxides of InAs via the following reaction:[25]

$$2\,Al(CH_3)_3 + In_2O_3 \longrightarrow 2\,In(CH_3)_3 + Al_2O_3, \quad (1)$$

$$2\,Al(CH_3)_3 + As_2O_3 \longrightarrow 2\,As(CH_3)_3 + Al_2O_3. \quad (2)$$

For TMA treated samples, a 1 s pulse of TMA is applied to the surface in the ALD chamber, followed by a 30 s purge with N_2 gas, at a 200 °C process temperature. This pulse cycle is repeated 18 times to maximize the reaction time, prior to the growth of the dielectric.

The second approach that we examine is the removal of surface oxides and the passivation of charged impurities at the surface via the application of an ArH plasma to the chip.[26,47,48] For this process, a remotely generated ArH plasma is applied to the surface of the samples for a total of 120 s before the growth of the dielectric layer. Atomic hydrogen is known to bond to As atoms and saturate the dangling bonds, passivating the surface.[26] A hydrogen plasma is also known to selectively remove the surface oxide via dry etching, again leading to an abrupt semiconductor–dielectric interface.[49,50]

In Fig. 3, we plot mobility as a function of density for each treatment, using samples taken from near the center of the wafer. The use of an ArH plasma in combination with oxide growth using TMA and H_2O as an oxidizer was found to increase the measured mobility relative to an untreated sample, showing the highest peak mobility for both near and far samples. In contrast, oversaturation with TMA causes a decrease in mobility compared to a single TMA exposure before Al_2O_3 growth. Finally, we note that the use of O_3 as a precursor does not seem to be effective for the creation of a clean dielectric interface—both ozone samples show a decreased quality relative to no treatment; however, the peak mobility shifts to a higher density. Measurements are taken on both samples near the center of the growth wafer (near) and samples taken far from the center of the growth wafer (far), across multiple measurement points and multiple cooldowns, as shown in Fig. 4. While there exists a significant difference in the mobility of

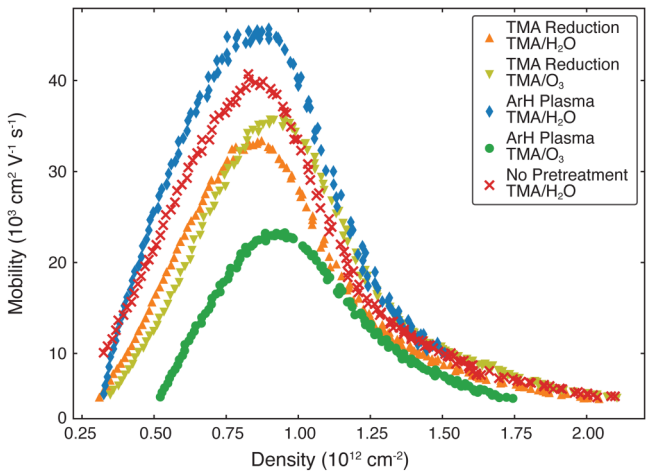

FIG. 3. Representative mobility vs density traces for each treatment, taken from samples near the center of the wafer. Samples oxidized with O_3 show a shifted peak mobility relative to those oxidized with H_2O. A peak mobility of 45 300 $cm^2/(V\,s)$ is extracted for a sample treated with a hydrogen plasma.

samples taken from different parts of the growth wafer, there remains a definite trend amongst similarly treated samples. The use of ArH plasma in combination with oxide growth using TMA and H_2O as an oxidizer results in a significant reduction in variance in mobilities for the highest quality samples.

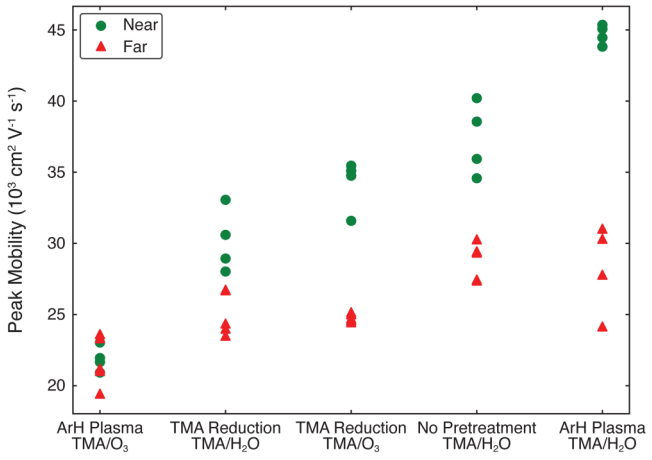

FIG. 4. Peak mobility achieved for different treatments and oxidizers. Measurements are made across different two samples, taken from near the center of the growth wafer (green) and from near the edge of the growth wafer (red), and at multiple locations on each Hall bar. Each point represents the peak mobility extracted from a sweep of gate voltage, as shown in red in Fig. 1(d), which were collected over multiple cooldowns, and at multiple measurement points.

IV. SCATTERING MECHANISMS

Finally, we turn to a detailed examination of scattering mechanisms across different density ranges and surface treatments. Unlike semiconductors such as GaAs where the Fermi level is pinned in the band gap, the location of the Fermi level in InAs has been shown to depend sensitively on surface states. Even in nominally undoped heterostructures, as is the case in this study, an electron density in the quantum well at zero gate voltage is induced by charged impurities at the surface.[44,51] As the concentration of charged impurities is decreased, the electron density in the quantum well at zero gate voltage is decreased toward zero. Figure 5 shows the density at zero gate voltage against the peak mobility. We observe an inverse relationship with the samples that have the highest mobility also having the lowest intrinsic electron density. Application of an ArH plasma is thus an effective method for terminating these charged impurities prior to dielectric growth.

In contrast, samples treated with TMA see either no significant change in the density of charged surface states or see an increase relative to no pre-treatment. Although the TMA treatment has been demonstrated to be effective in removing the surface oxide, such studies largely investigate the optical properties of the cleaned surface, using either x-ray photo-emission spectroscopy[45–47] or infrared spectroscopy,[52] rather than the electrical properties. We suggest that the inconsistency between previous studies and our result can be explained by the growth of an Al_2O_3 layer during the pre-treatment. This acts as a diffusion barrier at 200 °C and terminates the native oxide removal process before completion,[53] which in this case limits the effectiveness of the treatment.

To understand the reduced mobility observed when using ozone as the oxidizer in the ALD process, we examine the relationship between density and mobility when peak mobility is achieved (see the supplementary material for additional data). The peak mobility in O_3 samples is shifted toward higher densities compared

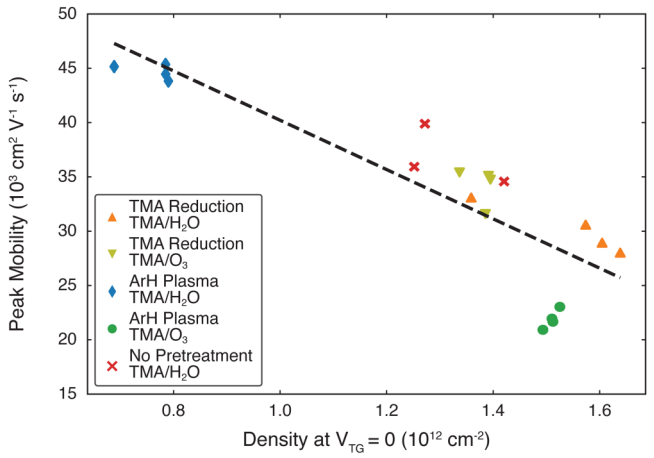

FIG. 5. Scatter plot of density at zero gate voltage against the peak mobility for samples taken near the center of the growth wafer. Samples with the lowest density at zero gate voltage have the highest measured peak mobility. The dashed black line is a linear fit and is a guide to the eye.

to those samples that use H_2O. Previous studies have found that the AlO_x grown by ozone is oxygen-rich relative to the optimal stoichiometry for aluminum oxide.[24,54] The increased incorporation of oxygen in the oxide will appear as remote charged impurity scatterers distributed throughout the dielectric,[35] and, therefore, a higher electron density has to be reached before these are fully screened.

V. CONCLUSION

In summary, we find scattering off charged surface impurities at the Al_2O_3 interface is a limiting factor in mobility in the current generation of shallow InAs quantum wells. For a quantum well 10 nm from the surface, the application of an ArH plasma prior to dielectric growth is effective in increasing the peak mobility to $\sim$45 300 cm^2/(V s) and reduces the variance in mobility compared to untreated samples or samples exposed to TMA saturation. For all samples, we find that the second subband is occupied at $V_{TG} = 0$ V. This is a complicating factor in the search for MZMs in InAs 2DEGs, as the formation of a greater number of 1D-subbands, as is likely with multiple occupied 2D-subbands, will generally lead to the formation of trivial Andreev bound states which can obscure signatures of MZMs.[3] For the current generation of samples, reaching the high-mobility limit with a small number of 1D-subbands will likely only be possible with a single occupied 2D-subband. Due to the pinning of the Fermi level in InAs, we find that a significant negative gate voltage will be necessary to tune into this regime.

SUPPLEMENTARY MATERIAL

See the supplementary material for a complete description of the fabrication, measurement and simulation setup, raw data for each surface treatment, and additional data showing the density at which peak mobility is achieved for different treatments.

ACKNOWLEDGMENTS

This research was supported by the Microsoft Corporation and the Australian Research Council Centre of Excellence for Engineered Quantum Systems (EQUS, No. CE170100009). The authors acknowledge the facilities as well as the scientific and technical assistance of the Research & Prototype Foundry Core Research Facility at the University of Sydney, part of the Australian National Fabrication Facility.

DATA AVAILABILITY

The data that support the findings of this study are available from the corresponding author upon reasonable request.

REFERENCES

[1]I. Žutić, J. Fabian, and S. Das Sarma, "Spintronics: Fundamentals and applications," Rev. Mod. Phys. **76**, 323–410 (2004).
[2]R. M. Lutchyn, J. D. Sau, and S. Das Sarma, "Majorana fermions and a topological phase transition in semiconductor-superconductor heterostructures," Phys. Rev. Lett. **105**, 077001 (2010).
[3]R. M. Lutchyn, E. P. A. M. Bakkers, L. P. Kouwenhoven, P. Krogstrup, C. M. Marcus, and Y. Oreg, "Majorana zero modes in superconductor–semiconductor heterostructures," Nat. Rev. Mater. **3**, 52–68 (2018).
[4]J. Shabani, M. Kjaergaard, H. J. Suominen, Y. Kim, F. Nichele, K. Pakrouski, T. Stankevic, R. M. Lutchyn, P. Krogstrup, R. Feidenhans'l, S. Kraemer, C. Nayak, M. Troyer, C. M. Marcus, and C. J. Palmstrøm, "Two-dimensional epitaxial superconductor-semiconductor heterostructures: A platform for topological superconducting networks," Phys. Rev. B **93**, 155402 (2016).
[5]V. Mourik, K. Zuo, S. M. Frolov, S. R. Plissard, E. P. A. M. Bakkers, and L. P. Kouwenhoven, "Signatures of Majorana fermions in hybrid superconductor-semiconductor nanowire devices," Science **336**, 1003–1007 (2012).
[6]S. M. Albrecht, A. P. Higginbotham, M. Madsen, F. Kuemmeth, T. S. Jespersen, J. Nygård, P. Krogstrup, and C. M. Marcus, "Exponential protection of zero modes in Majorana islands," Nature **531**, 206 (2016).
[7]F. Nichele, A. C. C. Drachmann, A. M. Whiticar, E. C. T. O'Farrell, H. J. Suominen, A. Fornieri, T. Wang, G. C. Gardner, C. Thomas, A. T. Hatke, P. Krogstrup, M. J. Manfra, K. Flensberg, and C. M. Marcus, "Scaling of Majorana zero-bias conductance peaks," Phys. Rev. Lett. **119**, 136803 (2017).
[8]H. J. Suominen, M. Kjaergaard, A. R. Hamilton, J. Shabani, C. J. Palmstrøm, C. M. Marcus, and F. Nichele, "Zero-energy modes from coalescing Andreev states in a two-dimensional semiconductor-superconductor hybrid platform," Phys. Rev. Lett. **119**, 176805 (2017).
[9]X.-L. Qi and S.-C. Zhang, "Topological insulators and superconductors," Rev. Mod. Phys. **83**, 1057–1110 (2011).
[10]A. Y. Kitaev, "Unpaired Majorana fermions in quantum wires," Physics-Uspekhi **44**, 131–136 (2001).
[11]C. Beenakker, "Search for Majorana fermions in superconductors," Ann. Rev. Condens. Matter Phys. **4**, 113–136 (2013).
[12]C. Nayak, S. H. Simon, A. Stern, M. Freedman, and S. Das Sarma, "Non-Abelian anyons and topological quantum computation," Rev. Mod. Phys. **80**, 1083–1159 (2008).
[13]J. D. Sau and S. Das Sarma, "Density of states of disordered topological superconductor-semiconductor hybrid nanowires," Phys. Rev. B **88**, 064506 (2013).
[14]S. Takei, B. M. Fregoso, H.-Y. Hui, A. M. Lobos, and S. Das Sarma, "Soft superconducting gap in semiconductor Majorana nanowires," Phys. Rev. Lett. **110**, 186803 (2013).
[15]W. Chang, S. M. Albrecht, T. S. Jespersen, F. Kuemmeth, P. Krogstrup, J. Nygård, and C. M. Marcus, "Hard gap in epitaxial semiconductor–superconductor nanowires," Nat. Nanotechnol. **10**, 232 (2015).
[16]M. Kjaergaard, F. Nichele, H. J. Suominen, M. P. Nowak, M. Wimmer, A. R. Akhmerov, J. A. Folk, K. Flensberg, J. Shabani, C. J. Palmstrøm, and C. M. Marcus, "Quantized conductance doubling and hard gap in a two-dimensional semiconductor–Superconductor heterostructure," Nat. Commun. **7**, 12841 (2016).
[17]H. Zhang, C.-X. Liu, S. Gazibegovic, D. Xu, J. A. Logan, G. Wang, N. van Loo, J. D. S. Bommer, M. W. A. de Moor, D. Car, R. L. M. Op het Veld, P. J. van Veldhoven, S. Koelling, M. A. Verheijen, M. Pendharkar, D. J. Pennachio, B. Shojaei, J. S. Lee, C. J. Palmstrøm, E. P. A. M. Bakkers, S. D. Sarma, and L. P. Kouwenhoven, "Quantized Majorana conductance," Nature **556**, 74 (2018).
[18]From 44 000 cm^2/(V s)[21] down to 1000 to 2000 cm^2/(V s).[16,54]
[19]A. C. Potter and P. A. Lee, "Engineering a $p + ip$ superconductor: Comparison of topological insulator and Rashba spin-orbit-coupled materials," Phys. Rev. B **83**, 184520 (2011).
[20]R. M. Lutchyn, T. D. Stanescu, and S. Das Sarma, "Momentum relaxation in a semiconductor proximity-coupled to a disordered s-wave superconductor: Effect of scattering on topological superconductivity," Phys. Rev. B **85**, 140513(R) (2012).
[21]K. S. Wickramasinghe, W. Mayer, J. Yuan, T. Nguyen, L. Jiao, V. Manucharyan, and J. Shabani, "Transport properties of near surface InAs two-dimensional heterostructures," Appl. Phys. Lett. **113**, 262104 (2018).
[22]A. T. Hatke, T. Wang, C. Thomas, G. C. Gardner, and M. J. Manfra, "Mobility in excess of 1×10^6 cm^2 v^{-1} s^{-1} in InAs quantum wells grown on lattice mismatched InP substrates," Appl. Phys. Lett. **111**, 142106 (2017).

[23]A. M. Whiticar, A. Fornieri, E. C. T. O'Farrell, A. C. C. Drachmann, T. Wang, C. Thomas, S. Gronin, R. Kallaher, G. C. Gardner, M. J. Manfra, C. M. Marcus, and F. Nichele, "Coherent transport through a Majorana island in an Aharonov–Bohm interferometer," Nat. Commun. **11**, 3212 (2020).
[24]M. Milojevic, F. S. Aguirre-Tostado, C. L. Hinkle, H. C. Kim, E. M. Vogel, J. Kim, and R. M. Wallace, "Half-cycle atomic layer deposition reaction studies of Al_2O_3 on $In_{0.2}Ga_{0.8}As$ (100) surfaces," Appl. Phys. Lett. **93**, 202902 (2008).
[25]S. Klejna and S. D. Elliott, "First-principles modeling of the 'clean-up' of native oxides during atomic layer deposition onto III-V substrates," J. Phys. Chem. C **116**, 643–654 (2012).
[26]G. Bell, N. Kaijaks, R. Dixon, and C. McConville, "Atomic hydrogen cleaning of polar III-V semiconductor surfaces," Surf. Sci. **401**, 125–137 (1998).
[27]J. D. Watson, "Growth of low disorder GaAs/AlGaAs heterostructures by molecular beam epitaxy for the study of correlated electron phases in two dimensions," Ph.D. thesis (Purdue University, 2015).
[28]H. Yamaguchi and Y. Horikoshi, "Step motion and as desorption on InAs (001) surfaces observed by scanning tunneling microscopy," Phys. Rev. B **48**, 2807–2810 (1993).
[29]S. J. Pauka, K. Das, J. M. Hornibrook, G. C. Gardner, M. J. Manfra, M. C. Cassidy, and D. J. Reilly, "Characterising quantum devices at scale with custom Cryo-CMOS," arXiv e-prints, arXiv:1908.07685 [physics.app-ph] (2019).
[30]S. Löhr, S. Mendach, T. Vonau, C. Heyn, and W. Hansen, "Highly anisotropic electron transport in shallow InGaAs heterostructures," Phys. Rev. B **67**, 045309 (2003).
[31]D. Ercolani, G. Biasiol, E. Cancellieri, M. Rosini, C. Jacoboni, F. Carillo, S. Heun, L. Sorba, and F. Nolting, "Transport anisotropy in $In_{0.75}Ga_{0.25}As$ two-dimensional electron gases induced by indium concentration modulation," Phys. Rev. B **77**, 235307 (2008).
[32]Y. Matsumoto and Y. Uemura, "Scattering mechanism and low temperature mobility of MOS inversion layers," Jpn. J. Appl. Phys. **13**, 367 (1974).
[33]J. P. Harrang, R. J. Higgins, R. K. Goodall, P. R. Jay, M. Laviron, and P. Delescluse, "Quantum and classical mobility determination of the dominant scattering mechanism in the two-dimensional electron gas of an AlGaAs/GaAs heterojunction," Phys. Rev. B **32**, 8126–8135 (1985).
[34]F. F. Fang, A. B. Fowler, and A. Hartstein, "Effective mass and collision time of (100) Si surface electrons," Phys. Rev. B **16**, 4446–4454 (1977).
[35]S. Das Sarma and E. H. Hwang, "Universal density scaling of disorder-limited low-temperature conductivity in high-mobility two-dimensional systems," Phys. Rev. B **88**, 035439 (2013).
[36]V. Umansky, R. de Picciotto, and M. Heiblum, "Extremely high-mobility two dimensional electron gas: Evaluation of scattering mechanisms," Appl. Phys. Lett. **71**, 683–685 (1997).
[37]H. Fu, K. V. Reich, and B. I. Shklovskii, "Surface roughness scattering in multi-subband accumulation layers," Phys. Rev. B **93**, 235312 (2016).
[38]C. Ellenberger, B. Simovič, R. Leturcq, T. Ihn, S. E. Ulloa, K. Ensslin, D. C. Driscoll, and A. C. Gossard, "Two-subband quantum Hall effect in parabolic quantum wells," Phys. Rev. B **74**, 195313 (2006).
[39]H. Störmer, A. Gossard, and W. Wiegmann, "Observation of intersubband scattering in a 2-dimensional electron system," Solid State Commun. **41**, 707–709 (1982).
[40]R. Fletcher, E. Zaremba, M. D'Iorio, C. T. Foxon, and J. J. Harris, "Evidence of a mobility edge in the second subband of an $Al_0.33Ga_0.67As$ – GaAs heterojunction," Phys. Rev. B **38**, 7866–7869 (1988).
[41]A. Troian, J. V. Knutsson, S. R. McKibbin, S. Yngman, A. S. Babadi, L. E. Wernersson, A. Mikkelsen, and R. Timm, "InAs-oxide interface composition and stability upon thermal oxidation and high-k atomic layer deposition," AIP Adv. **8**, 125227 (2018).
[42]G. Hollinger, R. Skheyta-Kabbani, and M. Gendry, "Oxides on GaAs and InAs surfaces: An x-ray-photoelectron-spectroscopy study of reference compounds and thin oxide layers," Phys. Rev. B **49**, 11159–11167 (1994).
[43]W. Wang, G. Lee, M. Huang, R. M. Wallace, and K. Cho, "First-principles study of GaAs(001)-β2(24) surface oxidation and passivation with H, Cl, S, F, and GaO," J. Appl. Phys. **107**, 103720 (2010).
[44]C. Affentauschegg and H. H. Wieder, "Properties of InAs/InAlAs heterostructures," Semicond. Sci. Technol. **16**, 708–714 (2001).
[45]H. D. Lee, T. Feng, L. Yu, D. Mastrogiovanni, A. Wan, T. Gustafsson, and E. Garfunkel, "Reduction of native oxides on GaAs during atomic layer growth of Al_2O_3," Appl. Phys. Lett. **94**, 222108 (2009).
[46]M. Tallarida, C. Adelmann, A. Delabie, S. van Elshocht, M. Caymax, and D. Schmeisser, "GaAs clean up studied with synchrotron radiation photoemission," IOP Conf. Ser. Mater. Sci. Eng. **41**, 012003 (2012).
[47]E. R. Cleveland, L. B. Ruppalt, B. R. Bennett, and S. Prokes, "Effect of an in situ hydrogen plasma pre-treatment on the reduction of GaSb native oxides prior to atomic layer deposition," Appl. Surf. Sci. **277**, 167–175 (2013).
[48]K. D. Choquette, R. S. Freund, M. Hong, H. S. Luftman, S. N. G. Chu, J. P. Mannaerts, and R. C. Wetzel, "Hydrogen plasma processing of GaAs and AlGaAs," J. Vac. Sci. Technol. B **11**, 2025–2032 (1993), https://avs.scitation.org/doi/pdf/10.1116/1.586538.
[49]R. P. H. Chang and S. Darack, "Hydrogen plasma etching of GaAs oxide," Appl. Phys. Lett. **38**, 898–899 (1981).
[50]A. Callegari, P. D. Hoh, D. A. Buchanan, and D. Lacey, "Unpinned gallium oxide/GaAs interface by hydrogen and nitrogen surface plasma treatment," Appl. Phys. Lett. **54**, 332–334 (1989).
[51]M. Noguchi, K. Hirakawa, and T. Ikoma, "Intrinsic electron accumulation layers on reconstructed clean InAs(100) surfaces," Phys. Rev. Lett. **66**, 2243–2246 (1991).
[52]W. Cabrera, M. D. Halls, I. M. Povey, and Y. J. Chabal, "Surface oxide characterization and interface evolution in atomic layer deposition of Al_2O_3 on InP (100) studied by in situ infrared spectroscopy," J. Phys. Chem. C **118**, 5862–5871 (2014).
[53]D. A. Henegar and P. T. Gougousi, "Comparison of the reactivity of alkyl and alkyl amine precursors with native oxide GaAs(100) and InAs(100) surfaces," Appl. Surf. Sci. **390**, 870–881 (2016).
[54]S. D. Elliott, G. Scarel, C. Wiemer, M. Fanciulli, and G. Pavia, "Ozone-based atomic layer deposition of alumina from TMA: Growth, morphology, and reaction mechanism," Chem. Mater. **18**, 3764–3773 (2006).